JOURNAL OF THE ROYAL SOCIETY Interface

Comparison of physical, chemical and cellular responses to nano- and micro-sized calcium silicate/poly(ε-caprolactone) bioactive composites

Jie wei, S.J Heo, D.H Kim, S.E Kim, Y.T Hyun and Jung-Woog Shin

J. R. Soc. Interface 2008 **5**, 617-630
doi: 10.1098/rsif.2007.1267

JOURNAL OF THE ROYAL SOCIETY Interface

J. R. Soc. Interface (2008) **5**, 617–630
doi:10.1098/rsif.2007.1267
Published online 13 November 2007

Comparison of physical, chemical and cellular responses to nano- and micro-sized calcium silicate/poly(ε-caprolactone) bioactive composites

Jie wei[1,2], S. J. Heo[1,3], D. H. Kim[1], S. E. Kim[3], Y. T. Hyun[3] and Jung-Woog Shin[1,*]

[1]*Team of BK21, First project team, Department of Biomedical Engineering, Inje University, Gimhae, Gyeongnam 621-749, Republic of Korea*
[2]*R&D Department, Taesan Solutions Ltd, Seoul 135-080, Republic of Korea*
[3]*Department of Future Technology, Korea Institute of Materials Science, Changwon, Gyeongnam 641-831, Republic of Korea*

In this study, we fabricated nano-sized calcium silicate/poly(ε-caprolactone) composite (n-CPC) and micro-sized calcium silicate/poly(ε-caprolactone) composite (m-CPC). The composition, mechanical properties, hydrophilicity and degradability of both n-CPC and m-CPC were determined, and *in vitro* bioactivity was evaluated by investigating apatite forming on their surfaces in simulated body fluid (SBF). In addition, cell responses to the two kinds of composites were comparably investigated. The results indicated that n-CPC has superior hydrophilicity, compressive strength and elastic modulus properties compared with m-CPC. Both n-CPC and m-CPC exhibited good *in vitro* bioactivity, with different morphologies of apatite formation on their surfaces. The apatite layer on n-CPC was more homogeneous and compact than on m-CPC, due to the elevated levels of calcium and silicon concentrations in SBF from n-CPC throughout the 14-day soaking period. Significantly higher levels of attachment and proliferation of MG63 cells were observed on n-CPC than on m-CPC, and significantly higher levels of alkaline phosphatase activity were observed in human mesenchymal stem cells (hMSCs) on n-CPC than on m-CPC after 7 days. Scanning electron microscopy observations revealed that hMSCs were in intimate contact with both n-CPC and m-CPC surfaces, and significantly cell adhesion, spread and growth were observed on n-CPC and m-CPC. These results indicated that both n-CPC and m-CPC have the ability to support cell attachment, growth, proliferation and differentiation, and also yield good bioactivity and biocompatibility.

Keywords: bioactivity; calcium silicate; cell proliferation and differentiation; nano- and micro-sized composites; poly(ε-caprolactone)

1. INTRODUCTION

Many studies have indicated that bioglass, glass ceramics and bioceramics containing CaO and SiO_2 possess a bone-like apatite-formation ability and exhibit good bioactivity as bone implant materials (Liu & Ding 2002; Xue *et al.* 2005). Bioactive $CaO–SiO_2$-based materials depend on the chemical reactivity of their materials in simulated body fluid (SBF) and bone-like apatite formation on their surfaces (Liu *et al.* 2001). Both Ca and Si ions are important to nucleation and growth of apatite, and influence the biological metabolism of osteoblastic cells, which are essential to the mineralization process and bone-bonding mechanism (Patricia *et al.* 2004). Previous research has suggested that silicon, an essential element in animal nutrition, could be localized in the active areas of young bone and could play an important role in bone metabolism (Liu *et al.* 2004*a–c*). Furthermore, the Si-containing ionic products from bioactive glass seem able to activate bone-related gene expression and stimulate osteoblast proliferation and differentiation (Xynos *et al.* 2000*a–c*). Therefore, silicon-containing bioactive materials have been paid special attention in recent years. For many years, researchers in the field of bone grafting have shown increasing interest in biocomposites of bioactive ceramics and biodegradable polymers, which appear to be more beneficial than conventional ceramic or polymer biomaterial alone (Marcolongo *et al.* 1997; Zhang & Ma 1999*a*,*b*). If properly designed, a composite should result in an implant exhibiting bioactivity and tailored physical,

*Author for correspondence (sjw@bme.inje.ac.kr).

Received 15 October 2007
Accepted 23 October 2007

biological and mechanical properties for specific biomedical applications (Li & Chang 2005*a*,*b*). To date, various biocomposites of biodegradable polymers, bioceramics and bioactive glasses have been used as bone generation materials with varying degrees of success (Du *et al.* 1997; Roether *et al.* 2002). Recently, researchers in the field of orthopaedics have placed considerable emphasis on developing bioactive composites of nano-ceramics and polymers (wherein nano-bioactive material particles are dispersed in suitable polymeric matrices) owing to their bone analogue design as well as their biological performance (Murugan & Ramakrishna 2005). Use of nano-sized particles is preferable because natural bone contains nano-sized crystallites, yielding a high mechanical strength. Filler particle size is an important characteristic that significantly influences mechanical properties as well as interactions between filler particles and the polymer matrix of composite materials (Wei *et al.* 2007). Additionally, well-dispersed nanoparticles with ultrafine structure in the composite have the potential for improved properties because their surfaces have minimal defects and a high surface area to volume ratio (Du *et al.* 1999; Ma & Zhang 1999). Use of micrometre-sized fillers does not yield incremental strength and is usually accompanied by reduced ductility and toughness (Weia & Ma 2004). Therefore, it should be possible to develop a satisfactory inorganic–organic nano-biocomposite using nano-sized bioactive ceramics to achieve these criteria.

Studies have recently proposed using calcium silicate (CS) biomaterials as new bone repair implants because these are proven to be bioactive, degradable and biocompatible; some studies have reported that CS in the form of powders, ceramics and plasma-sprayed coatings exhibited excellent *in vitro* and *in vivo* bioactivity (Liu *et al.* 2004; Ni *et al.* 2006). Other studies have incorporated CS into biodegradable polymers such as poly(lactic acid-*co*-glycolic acid) (PLGA), poly(3-hydroxybutyrate-*co*-3-hydroxyvalerate) (PHBV) and poly(D,L-lactic acid) (PLA) to fabricate bioactive composites, and results have shown that adding CS into polymers not only introduces bioactivity into a composite but can also improve the composite's mechanical properties and hydrophilicity (Li & Chang 2004, 2005*a*,*b*). Therefore, $CaSiO_3$ materials might be good candidates for addition during the preparation of bioactive composites.

To the best of our knowledge, no previous study has examined the addition of nano- (n-CS) and micro-sized calcium silicate (m-CS) into polymers during the preparation of composites (such as poly(ε-caprolactone), PCL). Moreover, no studies have compared the physicochemical properties of and *in vitro* cell responses to both n-CS/PCL composites (n-CPC) and m-CS/PCL composites (m-CPC). Determining whether bioactive nano-composites have properties superior to micro-composites, or whether nano-composites have some special properties due to their small size and huge surface area requires conducting *in vitro* comparative studies on both novel n-CPC and m-CPC. In addition, understanding how nano- and micro-sized materials in a polymer affect the physicochemical, bioactive and biocompatible properties of the resultant biocomposites could provide useful information to clarify how special properties differ between nano- and micro-sized composites, enabling design of superior bone implanted biomaterials. Therefore, we investigated the influences that nano- and micro-sized $CaSiO_3$ in PCL matrix had on mechanical properties, hydrophilicity, degradability and apatite formation in SBF, and the *in vitro* preliminary biocompatibility (such as cell attachment, growth, morphology, proliferation and differentiation) of both types of composite.

2. MATERIALS AND METHODS

2.1. Preparation of nano-$CaSiO_3$

We synthesized n-CS using a chemical precipitation method. This reaction used $Ca(NO_3)_2{\cdot}4H_2O$ and $Na_2SiO_3{\cdot}9H_2O$ as starting materials. The two reagents in a 1 : 1 stoichiometric proportion were dissolved in deionized water in beakers, and the concentration was adjusted to 0.5 mol l^{-1}; 0.2% (w/v) polyethylene glycol was added to 300 ml of $Ca(NO_3)_2$ solution at ambient temperature as a dispersant. The $Ca(NO_3)_2$ solution was stirred while 300 ml of Na_2SiO_3 solution was added. After the precipitation was complete, $CaSiO_3$ precipitate was obtained and fully washed with deionized water. The $CaSiO_3$ precipitate was then mixed in a solid-solution ratio of 1% (w/v) with dimethylformamide (DMF) in a three-neck flask; DMF was used as a dispersant to prevent the n-CS from aggregation. The mixture was stirred while the temperature was gradually increased to between 100 and 120°C to evaporate the water. The mixture was maintained at 120°C for 5 h and then cooled to room temperature. The resulting n-CS/DMF slurry was stored in a beaker until use. A portion of the n-CS slurry was vacuum-dried at room temperature to obtain n-CS powder samples. Another portion of the n-CS slurry was dried at 100°C for 12 h and sintered at 900°C for 2 h to obtain m-CS powder samples, after which it was ground and sieved to obtain particles between 10 and 50 µm for future use. Both the obtained n-CS and m-CS powders were then characterized for phase composition and surface morphology using X-ray diffraction (XRD; Geigerflex; Rigaku Co., Tokyo, Japan) and scanning electron microscopy (FE-SEM; S-4300SE; Hitachi Ltd, Tokyo, Japan).

2.2. Preparation of n-CP and m-CP composites

Because hydrothermally synthesized n-CS slurries dried in air agglomerate, reducing homogeneity, we used the n-CS/DMF slurry directly to prepare n-CS/PCL composite (n-CPC) with 40 wt% n-CS content, using a simple solvent-casting method. Briefly, PCL, supplied as pellets (M_w = 80 000; Sigma-Aldrich, St Louis, MO, USA) was dissolved in chloroform to a concentration of 20% (w/v), and a specific quantity of n-CS/DFM slurry (according to the produced composites with 40 wt% n-CS content) was added to the

Table 1. Ion concentrations of SBF in comparison with those of human blood plasma.

	ion concentrations (mM)							
types	Na^+	K^+	Mg^{2+}	Ca^{2+}	Cl^-	HCO^{3-}	HPO_4^{2-}	SO_4^{2-}
SBF	142.0	5.0	1.5	2.5	147.8	4.2	1.0	0.5
blood plasma	142.0	5.0	1.5	2.5	103.0	27.0	1.0	0.5

PCL/chloroform solution with continuous stirring for 2 h to ensure uniform dispersion of n-CS in the mixture. The mixture of n-CS/PCL/DFM/chloroform was heat-dried at 80°C for approximately 2 h to allow the chloroform to be fully evaporated, resulting in the n-CS/PCL/DMF mixture. Then, the mixture was stirred and its temperature was gradually increased to between 120 and 140°C and maintained for 2 h. The obtained mixture was cast into a $100\times100\times3\ mm^3$ Teflon mould, and the dense sample was air-dried in a fume hood for 24 h to evaporate DFM and subsequently vacuum-dried at 50°C for 48 h to remove any remaining solvent. After being fully washed using deionized water and ethanol, the product was dried at room temperature in a fume hood for 48 h. The obtained dense samples were cut into discs sized $10\times10\times3\ mm^3$ and stored in a dry vacuum desiccator until use.

The dense samples of m-$CaSiO_3$/PCL composite (m-CPC) with 40 wt% m-CS content were also prepared using a solvent-casting method. Briefly, PCL pellets were dissolved in chloroform with a concentration of 20% (w/v), and a specific quantity of m-$CaSiO_3$ powder (according to the produced composites with 40 wt% m-CS content) was added to the solution with continuous stirring for 2 h to ensure uniform dispersion of m-CS powder. The obtained mixture of m-CS/PCL/chloroform was cast into a $100\times100\times3\ mm^3$ Teflon mould. The subsequent procedure was similar to the method used to prepare the samples of n-CS/PCL composite.

To determine mechanical properties, hydrophilicity, degradation, apatite formation in SBF and surface morphology of n-CPC and m-CPC, composite dense samples were fabricated using the same method of solvent casting in a different Teflon mould. Surface morphology of the specimens was examined under a Hitachi S-4300SE FE-SEM.

2.3. Mechanical properties, degradability and hydrophilicity

The mechanical strength of n-CPC and m-CPC samples ($10\times10\times10\ mm^3$) was measured at room temperature using a compression test at a constant displacement rate of $2\ mm\ min^{-1}$. The jigs were specially designed to provide a uniform load on the composite samples, and a Bionix 858.20 (MTS Systems Corp., Eden Prairie, MN, USA) was used to conduct tests. The compressive strength and elastic modulus were calculated within the linear range of the stress–strain curve. For each composition, four to five specimens were tested and the results were averaged.

The weight loss in n-CPC and m-CPC specimens sized $10\times10\times3\ mm^3$ during degradation in phosphate-buffered saline (PBS; pH 7.4) solution was measured using changes in dry weight after incubation for a specified time period. For such tests, the specimens were removed, rinsed in distilled water and dried in a vacuum oven for one week. All the values presented are the average of three specimens. The percentage of weight loss was computed using the following equation:

$$\text{weight loss}(\%) = 100\times(W_0 - W_t)/W_0$$

where W_0 is the starting dry weight and W_t is the dry weight at time t.

Surface wettability of n-CPC and m-CPC specimens sized $10\times10\times3\ mm^3$ was determined by measuring the contact angle of water droplets on the surface of the various specimens using a contact angle measurement system (SEO 300A; Surface and Electro-Optics Co., Ansan, Korea). The water contact angle method was employed to determine polar interactions across the material–water interface. Each sample was mounted on the platform and a goniometer (Rame Hart, Mountain Lakes, NJ, USA) was aligned and focused on the material–air interface. A microsyringe (Perfektum; Popper & Sons, Inc., Tokyo, Japan) was used to form 10 µl water droplets, which were dropped onto three different surface points on each sample; water contact angles were measured after 30 s. The results presented here represent the mean ± s.d. of four to five contact angles per sample.

2.4. Soaking specimens in SBF and measuring the ionic concentration

In vitro bioactivity of n-CPC and m-CPC samples was evaluated by examining apatite formation on their surfaces in SBF. The SBF had ion concentrations similar to those found in human blood plasma, as discussed in Kokubo (1990). The SBF was prepared by dissolving reagent grade NaCl, $NaHCO_3$, KCl, $K_2HPO4{\cdot}3H_2O$, $MgCl_2{\cdot}6H_2O$, $CaCl_2$ and Na_2SO_4 in ion-exchanged distilled water. Table 1 presents the ion concentrations in the SBF solution and in human blood plasma; the solution was buffered at pH 7.4 with tris(hydroxymethyl)aminomethane ($(CH_2OH)_3CNH_2$) and 1 M HCl at 37°C.

Specimens sized $10\times10\times3\ mm^3$ were cut, polished with diamond paste, washed with distilled water, dried in a vacuum at room temperature and then immersed in 30 ml of the SBF at 37°C for 1, 3, 5, 7 and 14 days without stirring or refreshing the SBF solution. After immersion, specimens were removed from the SBF solution, gently rinsed with distilled water and dried at

room temperature. The morphology and composition of apatite that had formed on composite surfaces were monitored under a Hitachi S-4300SE FE-SEM with an energy-dispersive X-ray spectrometer (EDS). At each time point, ionic concentrations of calcium (Ca), phosphorus (P) and silicon (Si) in the SBF solution were measured using inductively coupled plasma atomic emission spectroscopy (ICP-AES).

2.5. Cell attachment, growth and proliferation

To investigate attachment and proliferation, n-CPC and m-CPC dense samples with a size of $10\times10\times3\ mm^3$ were sonicated in ethanol and sterilized using ultraviolet light. For cell adhesion experiments, MG63 cells (purchased from Korean Cell Line Bank, no. 21427, Korea) were seeded on the discs at a density of 2×10^3 cells per disc. Cells were allowed to adhere for 1 h before each well was gently flooded with 1 ml of medium. Cell attachment was determined using a 3-(4,5-dimethylthiazol-2-yl)-2,5-diphenyltetrazolium bromide (MTT) assay after incubation for 4 h. Cell proliferation was evaluated after seeding cells at a density of 2×10^3 cells per disc, followed by incubation for 1, 4 and 7 days, with the medium replaced every second day. Adhesion and viable cells on substrates were assessed quantitatively using the MTT assay. In brief, composite cell constructs were placed in a culture medium containing MTT and incubated in a humidified atmosphere at 37°C for 4 h. Cell growth was determined using the MTT assay (MTT Kit; Roche Diagnosis Corp., Indianapolis, IN, USA). The absorbance value was measured at 570 nm using a microplate reader. Six specimens were tested at each incubation period, and each test was performed in triplicate. Results are reported as OD units. The morphologies of cells cultured on both n-CPC and m-CPC samples were observed and photographed under an inverted light microscope (IMT-2, A10PL; Olympus, Tokyo, Japan).

2.6. Alkaline phosphatase activity

To evaluate alkaline phosphate (ALP) activity, 5×10^4 human mesenchymal stem cells (hMSCs; purchased from Cambrex Bio Science Walkersville, Inc., Walkersville, MD, USA) were seeded on the n-CPC and m-CPC dense samples with a size of $10\times10\times3\ mm^3$, and ALP activity was measured on days 1, 4 and 7. Prior to cell seeding, the scaffolds were soaked in 75% ethanol solution for 60 min and sterilized overnight under UV irradiation. The adherent cells were removed from composites and lysed with PBS; this procedure was followed by adding a cell lysis buffer containing 0.1% Triton X-100 to the samples and freezing them to −20°C. The frozen samples were thawed at 37°C for 5 min to measure ALP activity according to the manufacturer's instructions (ALP kit 104; Sigma). A 50 ml sample was mixed with 50 ml *p*-nitrophenol ($1\ mg\ ml^{-1}$) in a 1 M diethanolamine buffer containing 0.5 mM $MgCl_2$ (pH 9.8) and incubated at 37°C for 15 min on a bench shaker. The reaction was stopped by adding 25 ml of 3 N NaOH per 100 ml of reaction mixture. The number of cells was determined by measuring the DNA content using Quant-iT(tm) PicoGreen dsDNA reagent kits (Molecular Probes, Eugene, OR, USA). Sample DNA was quantified by measuring fluorescence with a Synergy HT Multi-Detection Microplate Reader (BioTek, Winooski, VT, USA) at wavelengths of 480 nm excitation and 520 nm emission. Enzyme activity was quantified by measuring absorbance at 405 nm, and ALP activity was calculated from a standard curve after normalizing to the total DNA content. The results are expressed in nanomoles of *p*-nitrophenol produced per minute per nanogram of DNA.

2.7. Cell morphology

hMSCs were used to evaluate biocompatibility of the n-CPC and m-CPC dense samples with a size of $10\times10\times3\ mm^3$. Approximately 50 µl of culture medium containing 5×10^4 cells was seeded on the top of the porous scaffolds which had previously been placed in 24-well culture plates. Cells were allowed to attach to substrates for 4 h, and then 1 ml of fresh culture medium was added to each well. Cells were incubated for 1, 4 and 7 days in a humidified atmosphere at 37°C and 5% CO_2. Cell morphology on composite was observed under a Hitachi S-4300SE FE-SEM. After the various culture times, sample cell constructs were washed twice with PBS solution and fixed with 4% formalin in PBS (pH 7.4) for 20 min. They were subsequently washed twice with PBS solution and dehydrated in a series of graded ethanol (50, 60, 70, 80, 90 and 100% v/v) for 3 min each. Finally, specimens were air-dried in a desiccator overnight. The dried specimens were glued onto copper specimen stubs, and sputter coated with gold prior to SEM observation.

2.8. Statistical analysis

Statistical analysis was performed using one-way ANOVA with *post hoc* tests. All results are expressed as the mean ± s.d. Differences were considered statistically significant at $p<0.05$.

3. RESULTS

3.1. Morphology of n-CS and m-CS

Figure 1 presents the SEM micrographs of n-CS and m-CS materials. Synthesized n-CS was uniformly needle-like, with powder agglomerating among the particles (figure 1*a*,*b*). This may have been due to the small particle size, with high surface energy resulting in their aggregation; n-CS aggregations were composed of needle-like grains approximately 50–90 nm in diameter and 100–350 nm in length. The transmission electron microscopy (TEM) micrographs show that the needle-like n-CS grains are approximately 10–30 nm in diameter and 100–250 nm in length (data not shown). Because hydrothermally synthesized n-CS slurries dried in air agglomerate, reducing homogeneity, we used the n-CS/DMF slurry directly to prepare n-CS/PCL composite, using a simple solvent-casting method.

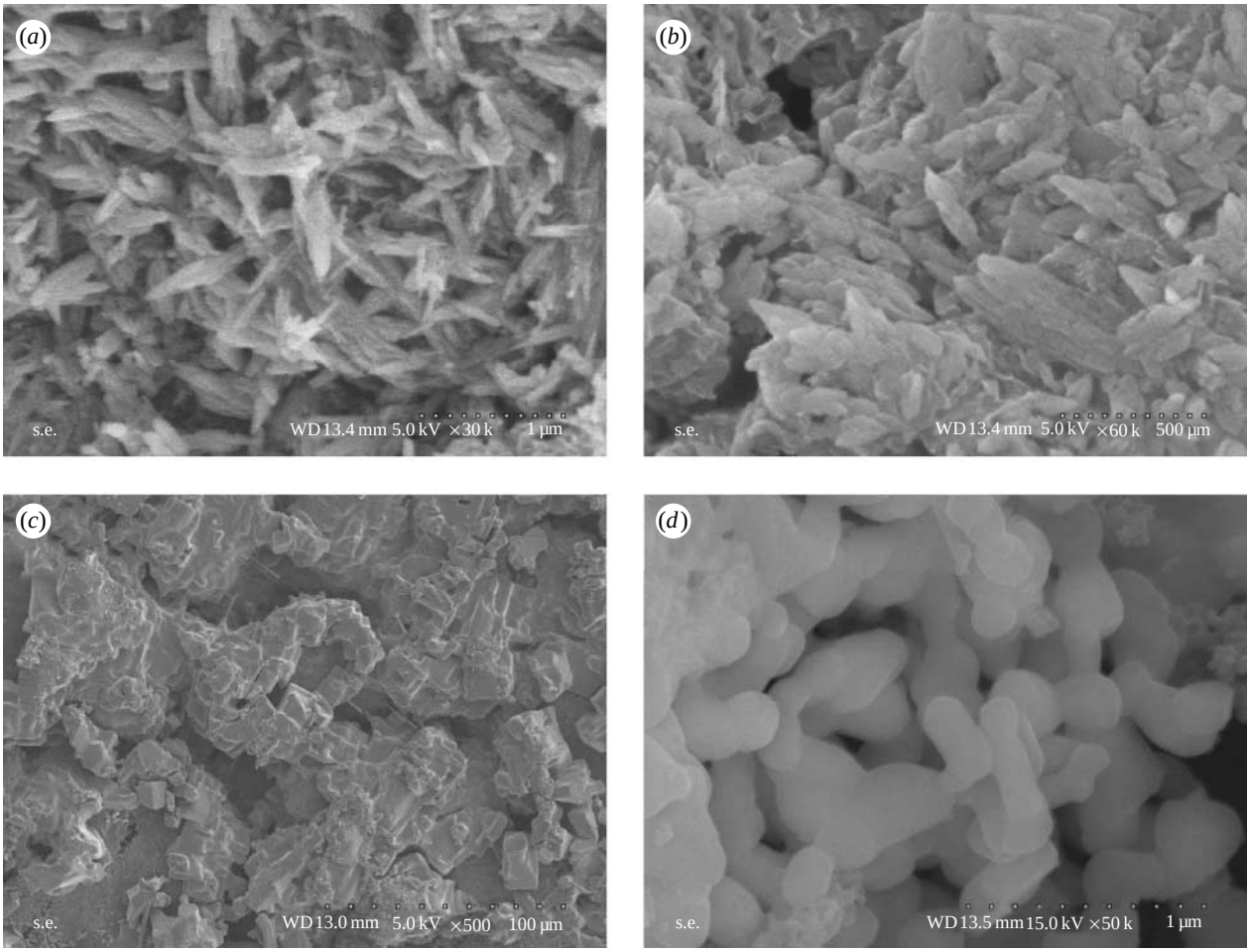

Figure 1. Scanning electron micrographs of (*a*,*b*) nano-calcium silicate and (*c*,*d*) micro-calcium silicate with different magnifications.

Figure 1*c*,*d* shows SEM micrographs of coarse m-CS particles with approximate elongated particle sizes of 20–50 µm. The differing morphologies resulted from difference in the powders' $CaSiO_3$ phases. Before heat treatment, powder particles were nano-sized, but after being heated to 900°C, n-CS crystallized, causing the particles to densify and become micro-sized grains.

3.2. XRD analysis of n-CS and m-CS

Figure 2 presents XRD patterns of n-CS and m-CS materials. Clearly, the XRD patterns of as-precipitated nano-$CaSiO_3$ powder trace depict only low peaks and background, indicating a state with low crystallinity (figure 2*b*). In contrast, powder after heat treatment at 900°C for 2 h exhibited numerous sharp peaks with high crystallinity (figure 2*a*). These results confirm that m-CS has greater crystallinity than n-CS and that all powders consisted of pure $CaSiO_3$ phase; no additional phase was identified within detectable limits.

3.3. Mechanical properties, hydrophilicity and degradability

Composite samples were not completely dense due to the processing method of solvent casting. Compressive strength and elastic modulus of both n-CPC and m-CPC samples increased with increasing CS content,

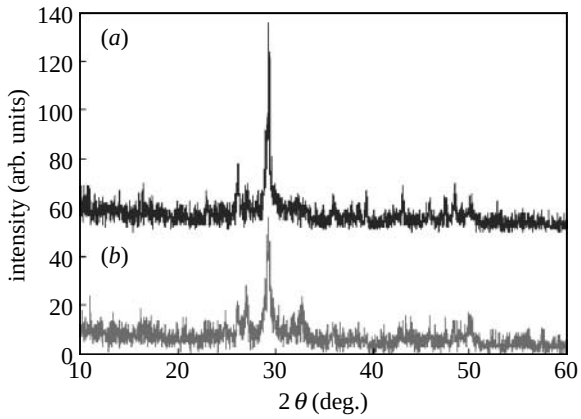

Figure 2. X-ray diffraction patterns of (*a*) n-CS and (*b*) m-CS.

and values were not significantly higher for n-CPC samples than m-CPC samples ($p<0.05$; table 2). The 40% (w/w) n-CS and m-CS composite samples exhibited the highest compressive strength (54 and 51 MPa, respectively) and elastic modulus (537 and 501 MPa, respectively), indicating that adding n-CS and m-CS to PCL improves mechanical properties to some degree. The highest values for n-CS and m-CS content (60%) corresponded to a lower compressive strength (37 and 35 MPa, respectively) and elastic modulus (246 and 235 MPa, respectively) than values of 40% ($p<0.05$; table 2), indicating that a critical concentration exists

Table 2. Mechanical properties of n-CPC and m-CPC with different CS contents (%); PCL as control; data represent the mean ± s.d., $n=5$.

	n-CPC		m-CPC	
samples	compressive strength (MPa)	elastic modulus (MPa)	compressive strength (MPa)	elastic modulus (MPa)
PCL	37 ± 2	191 ± 8	—	—
CS (20%)	43 ± 1	345 ± 21	40 ± 2	426 ± 12
CS (40%)	54 ± 1.5	537 ± 24	51 ± 1	501 ± 19
CS (60%)	37 ± 3	246 ± 12	35 ± 4	239 ± 9

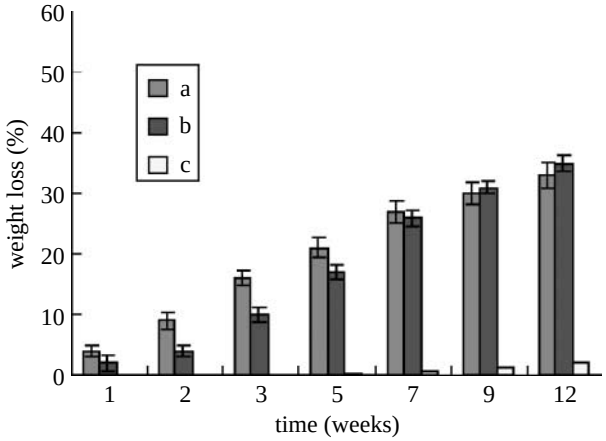

Figure 3. Change of weight loss of (a) n-CPC and (b) m-CPC with 40 wt% CS content in PBS at different incubated times and (c) pure PCL as a control. Data represent the mean ± s.d., $n=3$.

Table 3. Water contact angles of n-CPC and m-CPC with different CS contents (%); PCL as control; data represent the mean ± s.d., $n=5$.

	water contact angles (deg.)	
samples	n-CPC	m-CPC
PCL	77.5 ± 0.8	—
CS (20%)	59.2 ± 1.2	63.6 ± 1.0
CS (40%)	26.7 ± 0.9	32.6 ± 1.3
CS (60%)	0	0

beyond which additional n-CS and m-CS diminish a composite's mechanical properties.

Figure 3a, b presents weight loss in both n-CPC and m-CPC samples, respectively, as a function of incubation time in PBS. This figure reveals that weight loss in both types of samples increased with incubation time: 30 and 32% for n-CPC and m-CPC containing 40 wt% CS content after 12 weeks, respectively. Weight loss in n-CPC samples was significantly greater than m-CPC during the first seven weeks. Pure PCL samples exhibited no significant weight loss, losing only 2.1% of its initial weight at the end of the degradation experiment (12 weeks).

Table 3 presents measured water contact angles of sample surfaces. The table reveals that for both n-CPC and m-CPC specimens, water contact angles significantly

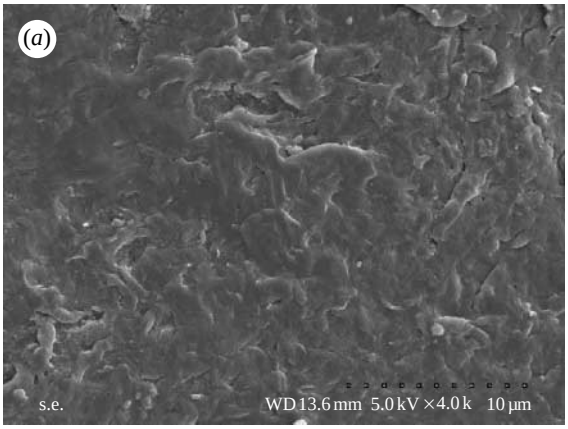

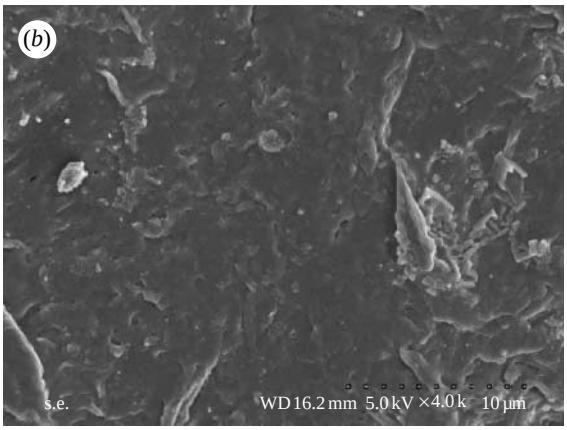

Figure 4. Scanning electron micrographs of the surface morphology of (*a*) n-CPC and (*b*) m-CPC before immersion in SBF.

decreased with increasing CS content ($p<0.01$; table 3), indicating improved hydrophilicity. Moreover, n-CPC had lower water contact angles than m-CPC at both 20 and 40% CS composite content, indicating that n-CPC had greater hydrophilicity than m-CPC.

3.4. Apatite formation in SBF

The *in vitro* bioactivity of n-CPC and m-CPC was investigated by soaking samples in SBF. Figure 4 shows the surface characteristics of n-CPC and m-CPC before soaking in SBF. This figure reveals that both types of specimens had coarse surfaces, but m-CPC had greater surface roughness than n-CPC and some debris also appeared on m-CPC (figure 4*b*). There are significant differences in surface morphology of the two kinds of samples between before and after soaking in SBF.

Figures 5 and 6 present SEM images of n-CPC and m-CPC surfaces after soaking in SBF for 14 days, after which both n-CPC and m-CPC surfaces exhibited typical spherical granules of apatite layers (figures 5*a* and 6*a*, respectively). Examination at greater magnifications (figures 5*b–d* and 6*b–d*) revealed that the granules contained many flake-like crystals with typical apatite morphology. These flake-like apatite crystals that had formed on both n-CPC and m-CPC surfaces had lengths of approximately 100–200 nm and widths of approximately 20–60 nm. Granules on the m-CPC specimen had a loosely packed apatite layer, whereas the apatite layer on the n-CPC specimen was densely

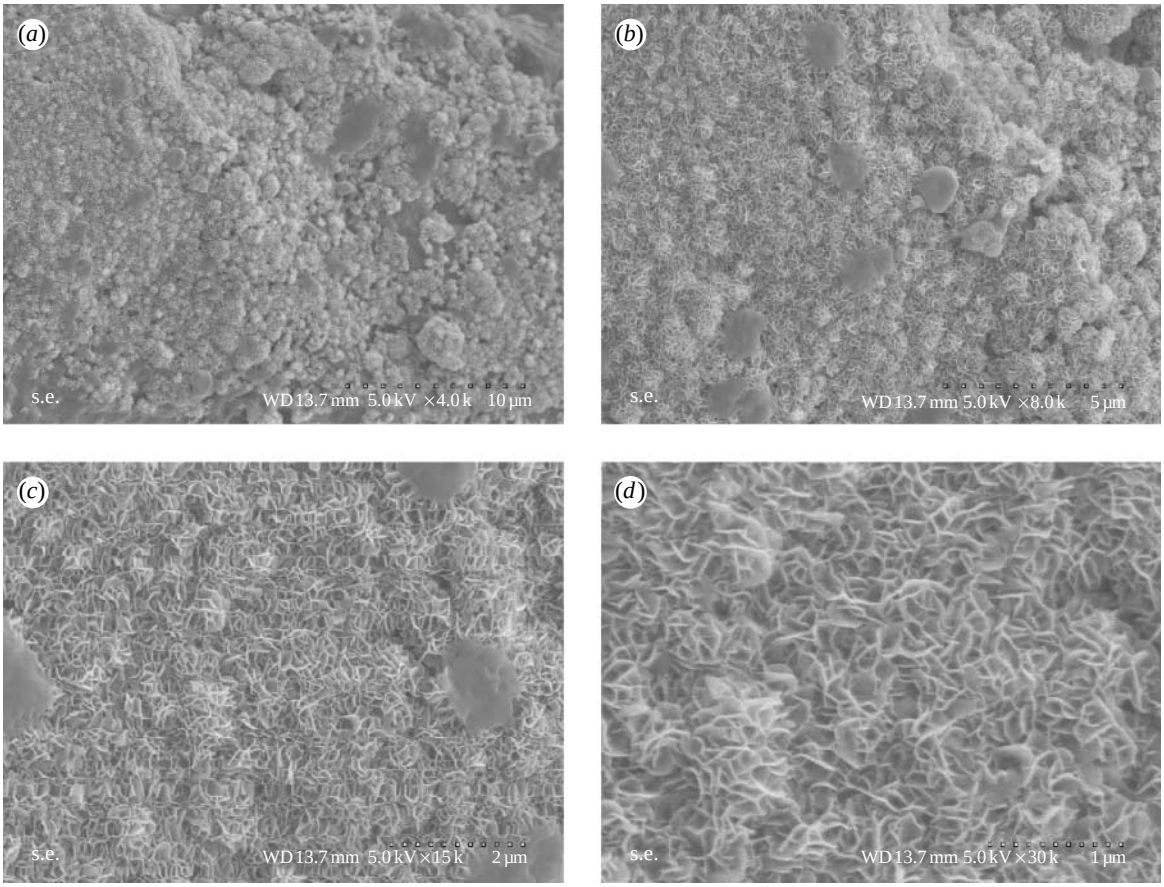

Figure 5. n-CPC specimens immersed in SBF for 14 days (*a–d*) at different magnifications.

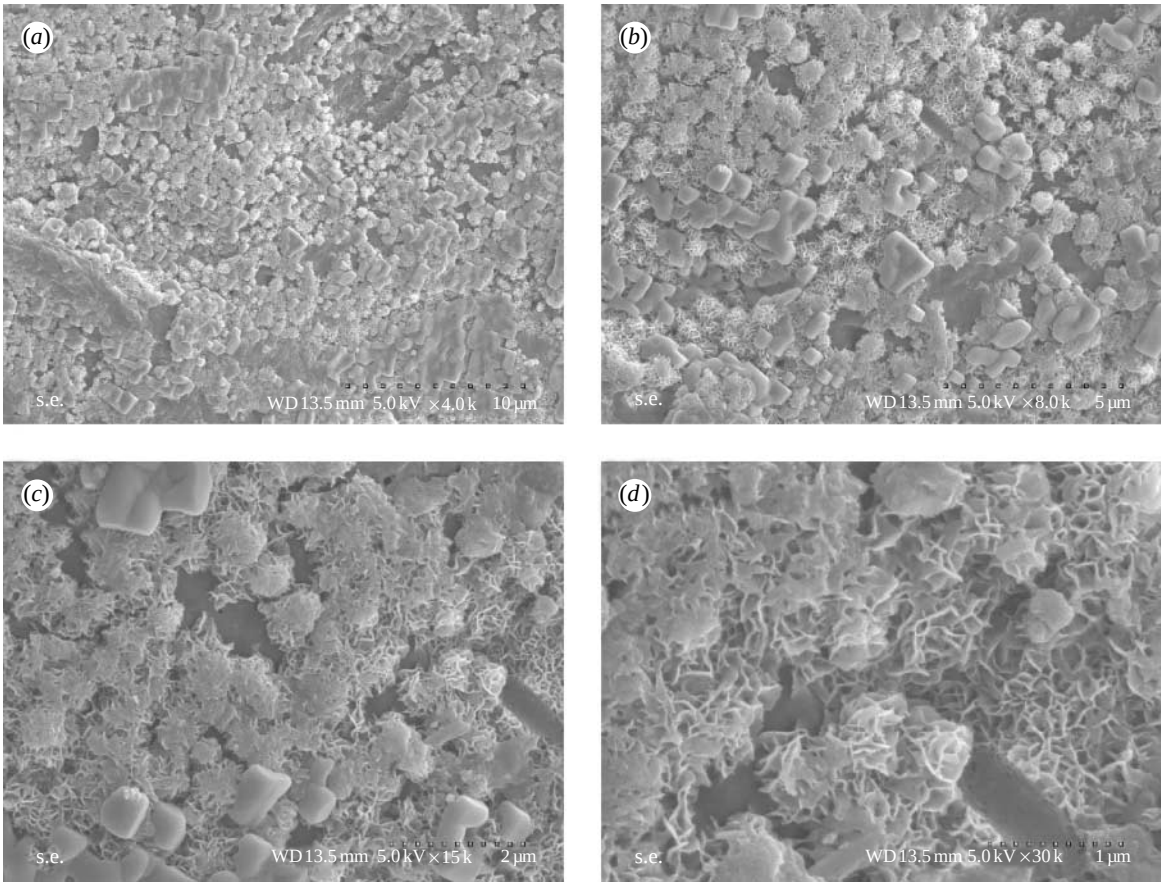

Figure 6. m-CPC specimens immersed in SBF for 14 days (*a–d*) at different magnifications.

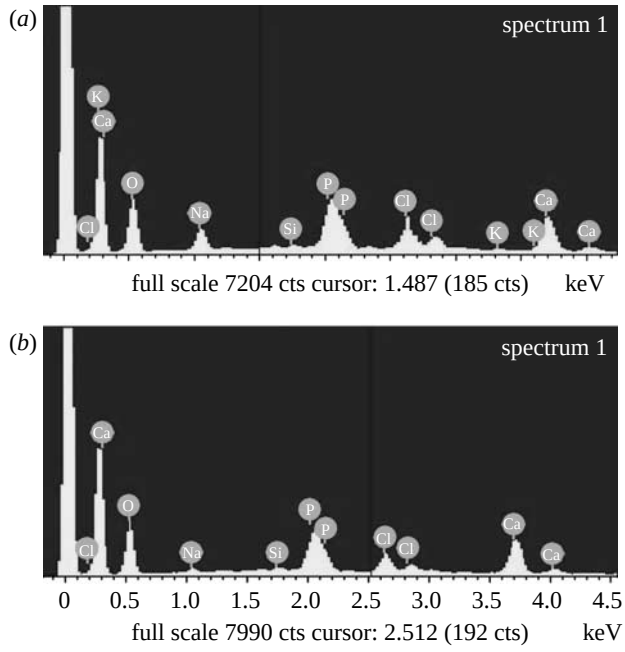

Figure 7. EDS spectra of surfaces of (*a*) n-CPC and (*b*) m-CPC samples in SBF for 14 days.

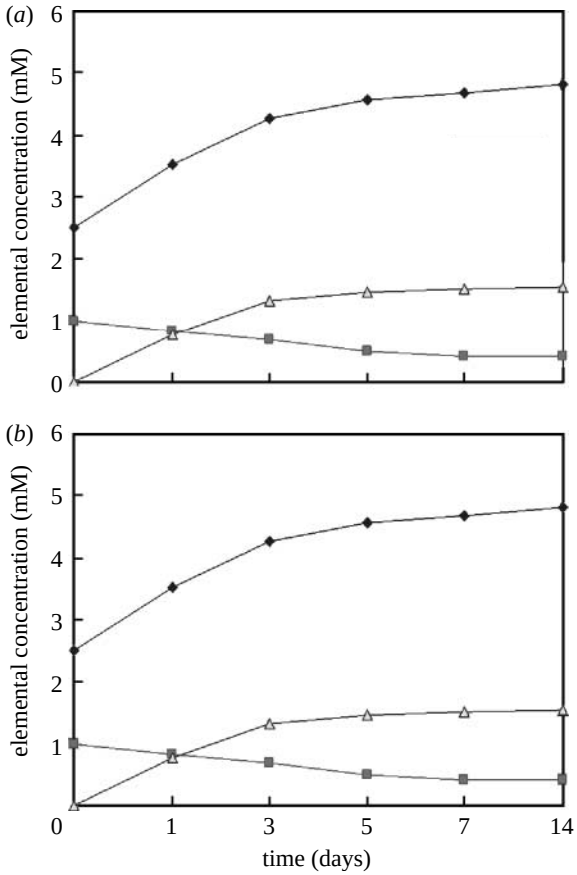

Figure 8. Concentration change of Ca, Si and P after immersion of (*a*) n-CPC and (*b*) m-CPC samples in SBF at different times (filled diamonds, Ca; filled squares, P; open triangles, Si).

packed. The crystalline layer of apatite on n-CPC was more compact and homogeneous than on m-CPC.

EDS spectra were examined for the apatite layers that formed on the composite surfaces after soaking in SBF for 14 days. Both Ca and P peaks were detected as shown in figure 7; Ca/P ratios for n-CPC and m-CPC specimens were 1.63 and 1.75, respectively, similar to the 1.67 Ca/P ratio of hydroxyapatite.

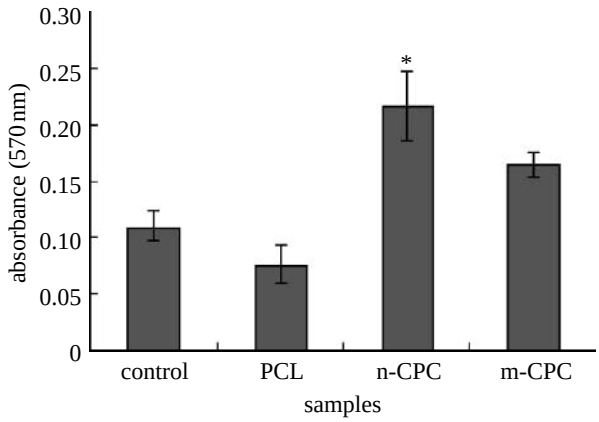

Figure 9. The early attachments of MG63 on n-CPC and m-CPC. In particular, the n-CPC showed a significantly higher value than the other group ($n=5$, $^*p<0.05$).

3.5. Ionic concentration change in SBF

Changes in the elemental concentrations of calcium, phosphorus and silicon were observed in the SBF solutions after the specimens were soaked for various periods (figure 8). In all specimens, calcium and silicon concentrations increased quickly up to 3 days, and thereafter, continued to increase at slower rates up to 14 days. In addition, n-CPC samples exhibited a more intensive release of both Ca and Si ions compared with m-CPC samples. In contrast to the increasing Ca and Si concentrations, P ion concentrations decreased gradually throughout the soaking period, and this decrease was more pronounced among n-CPC than m-CPC specimens.

3.6. Cell attachment

The MTT assay was used to assess the relative number of cells that adhered to the various materials because optical density absorbance values can be used as indicators of the relative number of cells on composites. Cell attachment was investigated using the MTT assay of MG63 cells cultured on pure PCL, m-CPC and n-CPC, and a tissue culture plate as a control. Figure 9 presents the results of cell attachment. After 4 h, n-CPC had significantly higher absorbance values than m-CPC, pure PCL or the control ($p<0.05$). These results indicate that cell attachment for n-CPC samples was superior to m-CPC samples, suggesting that n-CPC specimens facilitate cell adhesion on their surfaces and can promote cell growth.

3.7. Cell growth and proliferation

Proliferation of MG63 osteoblast-like cells cultured on both n-CPC and m-CPC samples was assessed using the MTT assay because OD values can provide an indication of cell growth and proliferation on various materials. Figure 10 reveals that OD values for n-CPC

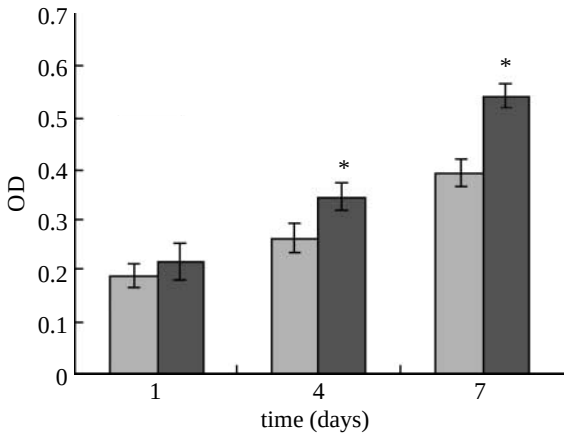

Figure 10. Proliferation of MG63 cells cultivated on m-CPC (light grey) and n-CPC (dark grey) for 1, 4 and 7 days. Data were represented as mean$\pm$s.d., $n=6$. Asterisks indicate that the proliferation rate of cells seeded on n-CPC was significantly higher than that of m-CPC at 4 and 7 days ($p<0.05$).

specimens were significantly higher than for m-CPC samples after 4 and 7 days ($p<0.05$); no significant differences appeared after 1 day. These results indicate that cell growth and proliferation (after 4 and 7 days) were superior in n-CPC specimens than in m-CPC specimens, suggesting that n-CPC facilitates cell growth and can promote cell proliferation.

Morphologies of MG63 cells cultured on n-CPC and m-CPC samples were observed using phase contrast microscopy, as shown in figure 11. The micrographs reveal that after being cultured for 1 and 4 days, cells on both n-CPC and m-CPC specimens grew well and stretched sufficiently, had full configurations and showed no abnormal plasma. After 7 days, the MG63 population increased manifestly, and cell proliferation was normal and fused into monolayer cells. These results indicate that both types of composites have no negative effect on cell morphology, viability or proliferation, and both provide good biocompatibility.

3.8. Cell differentiation

Cell differentiation was assessed in terms of ALP activity in hMSCs at 1, 4 and 7 days of culture, as shown in figure 12. At 1 and 4 days, ALP was expressed at lower levels, and no significant differences were detected between n-CPC and m-CPC samples. Subsequently, ALP activity increased with time. Cells on both n-CPC and m-CPC samples exhibited higher levels of ALP activity at 7 days than at 4 days, indicating that hMSCs differentiated most at 7 days. Moreover, at 7 days, ALP activity on n-CPC samples was significantly greater than on m-CPC samples ($p<0.05$).

3.9. Cell morphology

Figure 13 presents SEM micrographs showing the morphological features of hMSCs cultured on n-CPC and m-CPC specimens after 4 and 7 days, respectively. After 4 days, cells had extended and spread well, exhibiting intimate contact with composite surfaces. After 7 days, cells on both composite surfaces had spread well and formed a confluent layer with intimate contact to surfaces, and the spreading cells maintained physical contact with each other. There are no significant differences in morphology of cells on the composites between n-CPC and m-CPC.

4. DISCUSSION

During the past few years, considerable effort has been spent on researching the nanostructure processing of nanoscale materials and their composites in order to obtain ultrafine structures with physical, mechanical, chemical and biological properties superior to their microscale counterparts (Liou *et al.* 2004). Some studies have suggested that bioactive composites prepared at the nano-level could play important roles in various biomedical applications owing to their unique functional properties which could have a great impact on cell–biomaterial interactions (Murugan & Ramakrishna 2005). Bone is a typical example of a nano-composite, and nano-composite bone grafts are considered superior to graft processes using monolithic and micro-composite materials (Zhang & Ma 1999*a*,*b*; Ma & Zhang 2001).

In this study, both n-CPC and m-CPC samples exhibited increased compressive strength and elastic modulus with increased CS content; composites with 40 wt% CS content exhibited significantly higher values than composites with 20 and 60 wt% CS content, suggesting that a weight ratio of approximately 40% (w/w) is optimal. However, n-CPC did not exhibit significantly greater compressive strength and elastic modulus than m-CPC, suggesting that there were no obvious differences for mechanical strength between m-CPC and n-CPC by incorporation n-CS and m-CS into PCL matrix. Composites degraded in PBS, both n-CPC and m-CPC samples, and weight loss increased with incubation time. Weight loss was significantly greater in n-CPC samples than m-CPC samples during the first seven weeks, but no significant differences were observed from 9 to 12 weeks. These results indicate that n-CPC has a much faster degradation time than m-CPC during the initial stage owing to its composition, and structure, for example, low crystallinity, its small size and huge specific surface area. In contrast, pure PCL did not exhibit significant weight loss during incubation and lost only 2.1% of its initial weight by the end of the degradation experiment (12 weeks), indicating that the increased weight loss of composites might have resulted mainly from CS degradation.

In addition to mechanical and degradable properties, surface properties can greatly affect the performance of an implanted material. Incorporating both n-CS and m-CS materials markedly improved the hydrophilicity of the composites' water contact angles, and values were lower for n-CPC samples than for m-CPC samples. These results suggest that incorporating hydrophilic inorganic materials into hydrophobic polymers is a viable way to improve polymer hydrophilicity, and that n-CPC has significantly greater hydrophilicity than m-CPC. Webb *et al.* (1998) proposed that when material surfaces are exposed to dilute serum, more

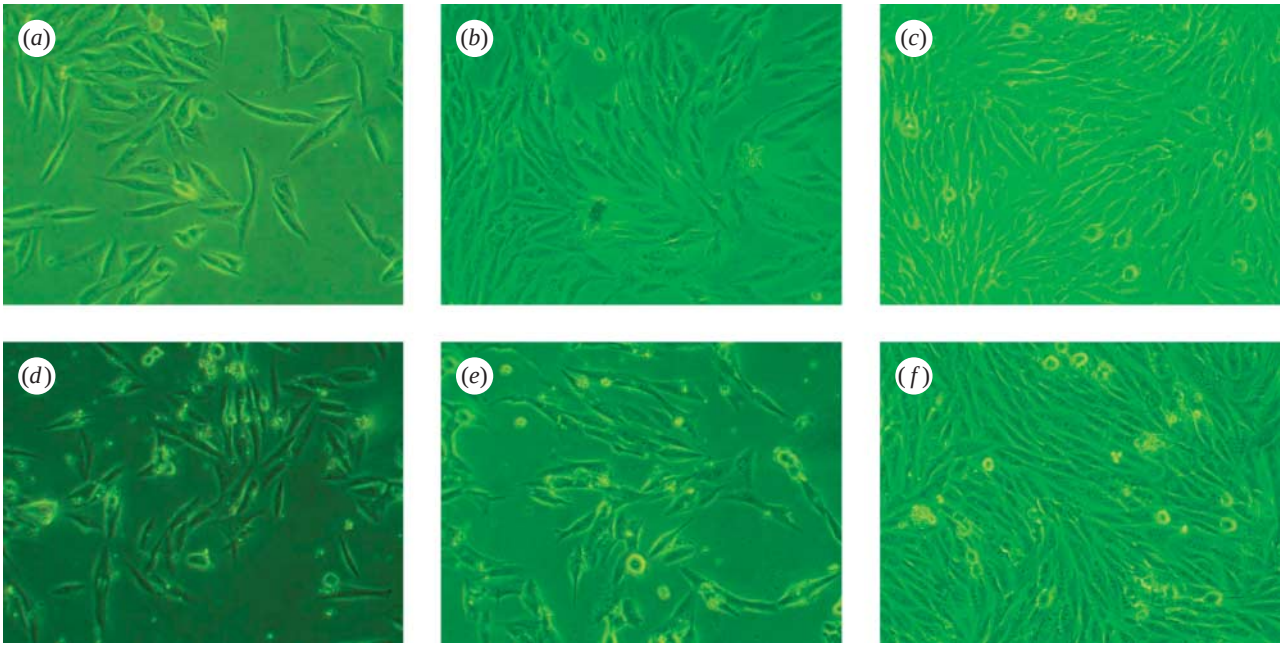

Figure 11. Phase contrast microscopy photographs of MG63 cells cultured on (*a–c*) n-CPC and (*d–f*) m-CPC at (*a,b*) 1 day, (*c,d*) 4 days and (*e,f*) 7 days.

hydrophilic surfaces are better for cell attachment, spreading and proliferation than hydrophobic surfaces. In addition, Yang *et al.* (2004) reported that a material's hydrophilicity aided absorption of fibronectin, which is essential for osteoblast adhesion *in vitro*. Therefore, the nano-composite's greater hydrophilic surface might be a more suitable area for cells to proliferate than that of micro-sized composites. Surface roughness is important to cell response, which directly affects osteoblast attachment, proliferation, differentiation, matrix synthesis and local factor production. This has been supported by numerous *in vitro* studies (Wennerberg *et al.* 1997). Differences in surface roughness affect adsorption of fibronectin and albumin *in vitro* influencing cell attachment and adhesion (Deligianni *et al.* 2001). In the present study, incorporation of n-CS and m-CS into PCL could significantly improve surface roughness of the composite surface as compared with PCL alone, which could promote the cell attachment and adhesion on the surfaces of the composites confirmed by cell culture experiments as shown in figure 8.

Ideally, an implanted material for bone regeneration is bioactive. A common feature of bioactive materials is their ability to bond to living bone through a bone-like apatite layer formed on their surface; this bone-like apatite plays an essential role in the formation, growth and maintenance of the tissue–biomaterial interface (Kokubo *et al.* 1990; Wu *et al.* 2006*a*,*b*). The results of this study revealed that both n-CPC and m-CPC can form apatite on their surfaces, suggesting that both types of composite are bioactive. The difference is that the crystalline layer of apatite on n-CPC samples was more homogeneous and compact than the layer on m-CPC samples, and apatite formation on n-CPC sample surfaces was faster and easier than on m-CPC samples throughout the 14-day soaking period. This

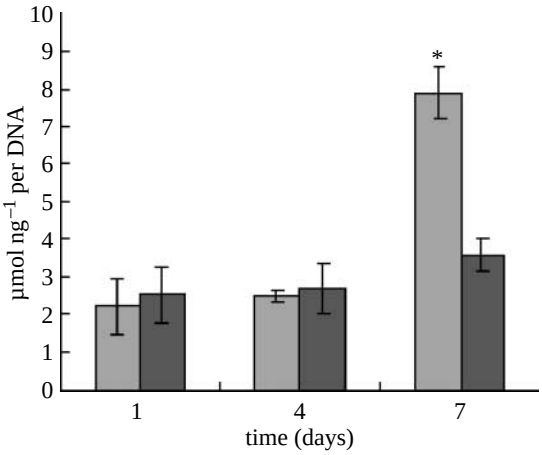

Figure 12. Alkaline phosphatase activity of hMSCs cultured on the n-CPC (light grey) and m-CPC (dark grey) samples for 1, 4 and 7 days. Alkaline phosphatase activity on n-CPC was significantly higher than that on m-CPC at 7 days ($n=5$, $^{*}p<0.05$).

might have occurred because n-CS particles were smaller than m-CS particles, resulting in a larger specific surface area when the composites were immersed in the SBF solution, promoting ion release. In addition, because nano-materials are not as stable as crystalline materials, the Ca–O bond was not as strong in n-CS as in the m-CS lattice. n-CS exhibited greater reactivity to the SBF solution than m-CS because Ca and Si ions were released easier and at a faster rate into the SBF solution, which might have resulted from differences between n-CS and m-CS microstructures and crystalline phases. Therefore, the relatively faster dissolution of n-CS might have increased local calcium concentration in the SBF, resulting in differing apatite-forming rates, morphology and Ca/P ratio in apatite precipitation. P ion concentration in the SBF decreased gradually throughout the entire soaking period; this

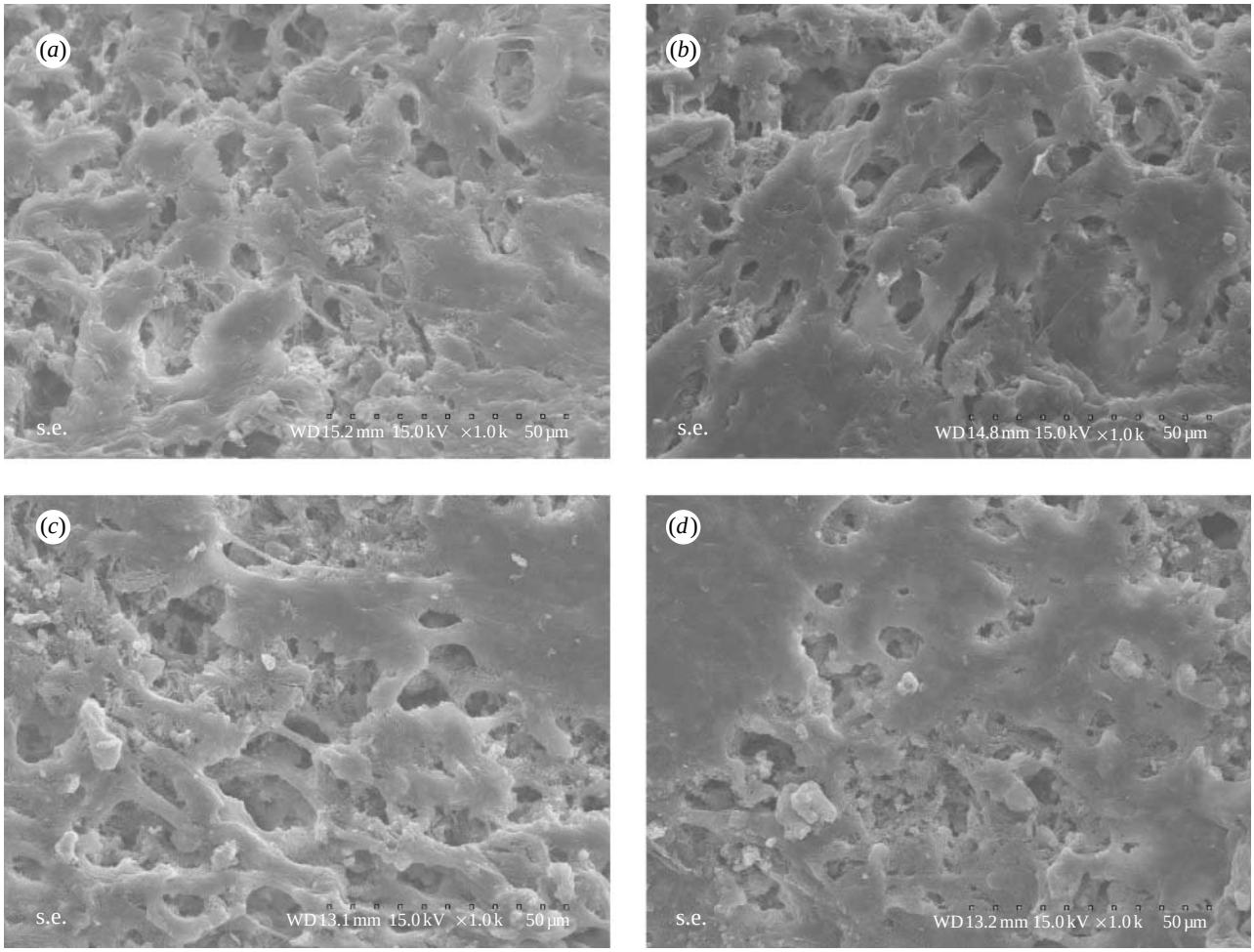

Figure 13. SEM micrographs of hMSCs seeded on the surfaces of the (*a*,*b*) n-CPC and (*c*,*d*) m-CPC at (*a*,*c*) 4 days and (*b*,*d*) 7 days.

decrease was probably due to the formation of amorphous calcium phosphate and the subsequent formation of apatite, which indirectly indicated that a precipitation reaction had occurred (Liu *et al.* 2002, 2004; Zhao & Chang 2005).

Cellular response and behaviour can be influenced by the characteristics of material surfaces *in vitro* (Ni *et al.* 2007). Attachment is part of the first phase of cell–material interactions, and the quality of this first phase will influence the cell's capacity for growth, morphology, proliferation and differentiation upon contact with the implant (Keeting *et al.* 2002; Liu & Ding 2003). The experimental cell attachment results of this study indicated that MG63 osteoblast-like cells adhered better to n-CPC than to m-CPC, PCL or the tissue culture plate within the first 4 h of culture. The superior ability of MG63 cells to attach to n-CPC compared with m-CPC is probably associated with differing material surface features, particle sizes, surface adsorbability, crystal structures, crystallinity and the dissolution product concentration between n-CPC and m-CPC. The nano-sized CS may have additional special surface properties, which promote cell attachment, and the more hydrophilic surface of n-CPC may be more useful for cell adhesion than that of m-CPC. Webster *et al.* (1999) reported a significant increase in protein adsorption and osteoblast adhesion on nano-sized ceramic materials compared to traditional micrometre-sized ceramic materials.

Cellular responses to a material, such as attachment, growth, proliferation and differentiation, depend not only on physical status but also on the material's chemical composition (Chou *et al.* 1998). Because various chemical compositions play a crucial role in determining cell response, they affect the quantity of ions released from a material and the consequent cell–material interaction (Wu *et al.* 2006*a*,*b*). Some studies have reported that ionic dissolution products containing Ca and Si from bioactive glasses can stimulate osteoblast proliferation and gene expression (Maeno *et al.* 2005). Xynos *et al.* (2000) showed that ionic products, Si and Ca in particular, could stimulate osteoblast proliferation. In the present study, the ICP results revealed that Si and Ca ions could be released from the composites in SBF, and that n-CPC resulted in a more rapid increase of Ca and Si ion concentrations than m-CPC, providing a higher basic ion concentration in the SBF solution. Moreover, MTT tests revealed that both n-CPC and m-CPC significantly stimulated MG63 osteoblast-like cell growth and proliferation over time, and that the n-CPC samples exhibited significantly increased cell growth and proliferation than m-CPC samples. The continuous dissolution associated with

the composites produced a calcium- and silicon-rich environment that might be responsible for stimulating cell growth and proliferation.

Besides proliferation, the ability of the osteoblasts to differentiate materials also indicates cell viability and indirectly shows that the materials are biocompatible (Sun *et al.* 2006). ALP activity has been used as an early marker for functionality and differentiation of osteoblasts during *in vitro* experiments (Xynos *et al.* 2000). In this study, hMSCs ALP activity on n-CPC exhibited significantly higher levels of expression than those on m-CPC at 7 days, indicating that cells differentiated more quickly after being cultured on n-CPC than on m-CPC. Therefore, the most distinct advantage of n-CPC appears to be the superior ALP activity compared with m-CPC. This increased activity probably resulted from the released Si and Ca ions, which might be responsible for stimulating cell proliferation and differentiation, suggesting that n-CPC may stimulate hMSC proliferation better than m-CPC.

Cell adhesion, spread and morphology are involved in various natural phenomena such as embryogenesis, maintenance of tissue structure, wound healing, immune response and metastasis, as well as tissue integration with biomaterials (Liu *et al.* 2006). The bioactivity and biocompatibility of biomaterials are very closely related to the behaviour of cells in contact with them and particularly to cell adhesion to their surface (Vrouwenvelder *et al.* 1992). This study's experimental SEM results indicated that hMSCs grew and proliferated and possessed good morphology, with abundant dorsal ruffles and filapodia, on n-CPC and m-CPC samples. The reason for this could be the local chemical environment due to the dissolution of n-CS and m-CS in the composites. In addition, the process of cell spreading is influenced by the underlying substrates, and some studies have indicated that the appearance of the bioactive layer (bone-like apatite layer that forms on a composite surface) influences the behaviour and morphology of osteoblasts cultured on the material's surface (Olmo *et al.* 2003). This suggests that the surface of n-CPC and m-CPC has the ability to form the apatite that is favourable for cell adhesion and growth, which implies good biocompatibility.

5. CONCLUSIONS

In this study, n-CPC and m-CPC composites were fabricated and physicochemical and biological properties of the two kinds of biocomposites were comparatively investigated for the first time. The results indicated that n-CPC had significantly greater hydrophilicity, compressive strength and elastic modulus than m-CPC. Both n-CPC and m-CPC exhibited good *in vitro* bioactivity with apatite formation on their surfaces in a SBF solution and good degradability in PBS. The apatite layer on n-CPC was more homogeneous and compact than on m-CPC throughout the 14-day soaking period. In addition, n-CPC and m-CPC exhibited differing surface morphologies of apatite formation, and n-CPC exhibited significantly greater weight loss than m-CPC during the first seven weeks, which might have been caused by differences between n-CS and m-CS microstructure, crystalline phase and dissolution in the composites because crystallinity was greater in m-CS than in n-CS.

MTT results indicated that both n-CPC and m-CPC had good bioactivity and biocompatibility. The attachment, growth and proliferation of MG63 cells were significantly better on n-CPC surfaces than on m-CPC surfaces. Results indicated that hMSC ALP activity expressed significantly higher levels of expression on n-CPC than on m-CPC after 7 days, indicating that cells cultured on the n-CPC differentiated better than cells on the m-CPC. SEM results revealed that hMSCs adhered well on the composites and proliferated with increased culture time, and that n-CPC and m-CPC surfaces exhibited good hMSC adhesion, spread and proliferation. In summary, the n-$CaSiO_3$/PCL composite exhibited superior mechanical properties, hydrophilicity, *in vitro* bioactivity and cell response than its microscale counterpart. These findings suggest that n-CPC is more bioactive than m-CPC and could be applied as a bone implant material.

This study was supported by the Fundamental Research Program of Korea Institute of Machinery and Materials.

REFERENCES

Chou, L., Al-Bazie, S., Cottrell, D., Giordano, R. & Nathason, D. 1998 Atomic and molecular mechanisms underlying the osteogenic effects of Bioglass materials. *Bioceramics* **11**, 265–268.

Deligianni, D. D., Katsala, N., Ladas, S., Sotiropoulou, D., Amedee, J. & Missirlis, Y. F. 2001 Effect of surface roughness of the titanium alloy Ti–6Al–4V on human bone marrow cell response and on protein adsorption. *Biomaterials* **22**, 1241–1251. (doi:10.1016/S0142-9612(00)00274-X)

Du, C., Cui, F. Z., Feng, Q. L., Zhu, X. D. & de Groot, K. 1997 Tissue response to nano-hydroxyapatite/collagen composite implants in marrow cavity. *J. Biomed. Mater Res.* **42**, 540–548. (doi:10.1002/(SICI)1097-4636(19981215)42:4<540::AID-JBM9>3.0.CO;2-2)

Du, C., Cui, F. Z., Zhu, X. D. & de Groot, K. 1999 Three-dimensional nano-HAp/collagen matrix loading with osteogenic cells in organ culture. *J. Biomed. Mater. Res.* **44**, 407–415. (doi:10.1002/(SICI)1097-4636(19990315)44:4<407::AID-JBM6>3.0.CO;2-T)

Keeting, P. E., Wiegand, K. E., Spelssberg, T. C. & Riggs, B. L. 2002 A novel silicon-containing osteotropic agent, zeolite A, induces proliferation and differentiation of normal human osteoblastlike cells. In *American Society for Bone and Mineral Research Annual Meeting, Atlanta, GA*, abstract 184.

Kokubo, T. 1990 Surface chemistry of bioactive glass-ceramics. *J. Non-Cryst. Solids* **120**, 138–157. (doi:10.1016/0022-3093(90)90199-V)

Kokubo, T., Ito, S., Huang, Z., Hayashi, T., Sakka, S., Kitsugi, T. & Yamamuro, T. 1990 Ca–P rich layer formed on high-strength bioactive glass-ceramic A–W. *J. Biomed. Mater. Res.* **24**, 331–343. (doi:10.1002/jbm.820240306)

Li, H. & Chang, J. 2004 Preparation and characterization of bioactive and biodegradable Wollastonite/poly(D,L-lactic acid) composite scaffolds. *J. Mater. Sci. Mater. Med.* **15**, 1089–1095. (doi:10.1023/B:JMSM.0000046390.09540.c2)

Li, H. & Chang, J. 2005*a* *In vitro* degradation of porous degradable and bioactive PHBV/wollastonite composite scaffolds. *Polym. Degrad. Stab.* **87**, 301–307. (doi:10.1016/j.polymdegradstab.2004.09.001)

Li, H. & Chang, J. 2005*b* pH-compensation effect of bioactive inorganic fillers on the degradation of PLGA. *Compos. Sci. Technol.* **65**, 2226–2232. (doi:10.1016/j.compscitech.2005.04.051)

Liou, S., Chena, S., Lee, H. & Bow, J. 2004 Structural characterization of nano-sized calcium deficient apatite powders. *Biomaterials* **25**, 189–196. (doi:10.1016/S0142-9612(03)00479-4)

Liu, X. & Ding, C. 2002 Plasma sprayed wollastonite/TiO_2 composite coating on titanium alloys. *Biomaterials* **23**, 4065–4077. (doi:10.1016/S0142-9612(02)00143-6)

Liu, X. & Ding, C. 2003 Plasma-sprayed wollastonite 2M/ZrO_2 composite coating. *Sur. Coat. Technol.* **172**, 270–278.

Liu, X., Ding, C. & Wang, Z. 2001 Apatite formed on the surface of plasma-sprayed wollastonite coating immersed in simulated body fluid. *Biomaterials* **22**, 2007–2012. (doi:10.1016/S0142-9612(00)00386-0)

Liu, X., Tao, S. & Ding, C. 2002 Bioactivity of plasma sprayed dicalcium silicate coatings. *Biomaterials* **23**, 963–968. (doi:10.1016/S0142-9612(01)00210-1)

Liu, X., Chuanxian, D. & Chu, P. K. 2004*a* Mechanism of apatite formation on wollastonite coatings in simulated body fluids. *Biomaterials* **25**, 1755–1761. (doi:10.1016/j.biomaterials.2003.08.024)

Liu, X., Poon, R. W. Y., Kwok, S. C. H., Chu, P. K. & Ding, C. 2004*b* Plasma surface modification of titanium for hard tissue replacements. *Sur. Coat. Technol.* **186**, 227–233. (doi:10.1016/j.surfcoat.2004.02.045)

Liu, X., Fu, R. K. Y., Poon, R. W. Y., Chen, P., Chu, P. K. & Ding, C. 2004*c* Biomimetic growth of apatite on hydrogen-implanted silicon. *Biomaterials* **25**, 5575–5581. (doi:10.1016/j.biomaterials.2004.01.015)

Liu, X., Huang, A., Ding, C. & Chu, P. K. 2006 Bioactivity and cytocompatibility of zirconia (ZrO_2) films fabricated by cathodic arc deposition. *Biomaterials* **27**, 3904–3911. (doi:10.1016/j.biomaterials.2006.03.007)

Ma, P. X. & Zhang, R. 1999 Synthetic nano-scale fibrous extracellular matrix. *J. Biomed. Mater. Res.* **46**, 60–72. (doi:10.1002/(SICI)1097-4636(199907)46:1<60::AID-JBM7>3.0.CO;2-H)

Ma, P. X. & Zhang, R. 2001 Micro-tubular architecture of biodegradable polymer scaffolds. *J. Biomed. Mater. Res.* **56**, 469–477. (doi:10.1002/1097-4636(20010915)56:4<469::AID-JBM1118>3.0.CO;2-H)

Maeno, S., Niki, Y., Matsumoto, H., Morioka, H., Yatabe, T., Funayama, A., Toyama, Y., Taguchi, T. & Tanaka, J. 2005 The effect of calcium ion concentration on osteoblast viability, proliferation and differentiation in monolayer and 3D culture. *Biomaterials* **26**, 4847–4855. (doi:10.1016/j.biomaterials.2005.01.006)

Marcolongo, M., Ducheyne, P. & Course, W. C. 1997 Surface reaction layer formation in vitro on a bioactive glass fiber/polymeric composite. *J. Biomed. Mater. Res.* **37**, 440–448. (doi:10.1002/(SICI)1097-4636(19971205)37:3<440::AID-JBM15>3.0.CO;2-F)

Murugan, R. & Ramakrishna, S. 2005 Development of nanocomposites for bone grafting. *Compos. Sci. Technol.* **65**, 2385–2406. (doi:10.1016/j.compscitech.2005.07.022)

Ni, S., Chang, J. & Chou, L. 2006 A novel bioactive porous $CaSiO_3$ scaffold for bone tissue engineering. *J. Biomed. Mater. Res. A* **76**, 196–205.

Ni, S., Chang, J., Chou, L. & Zhai, W. 2007 Comparison of osteoblast-like cell responses to calcium silicate and tricalcium phosphate ceramics *in vitro*. *J. Biomed. Mater. Res. B: Appl. Biomater.* **80**, 174–183.

Olmo, N., Martin, A. I., Salinas, A. J., Turnay, J., Vallet-Regi, M. & Antonia Lizarbe, M. 2003 Bioactive sol–gel glasses with and without a hydroxycarbonate apatite layer as substrates for osteoblast cell adhesion and proliferation. *Biomaterials* **24**, 3383–3393. (doi:10.1016/S0142-9612(03)00200-X)

Patricia, V., Marivalda, M. P., Alfredo, M. G. & Fatima, L. 2004 The effect of inonic products from bioactive glass dissolution on osteoblast proliferation and collagen production. *Biomaterials* **25**, 2941–2948. (doi:10.1016/j.biomaterials.2003.09.086)

Roether, J. A., Boccaccini, A. R., Hench, L. L., Maquet, V., Gautier, S. & Jerjme, R. 2002 Development and *in vitro* characterization of novel bioresorbable and bioactive composite materials based on polylactide foams and Bioglass® for tissue engineering applications. *Biomaterials* **23**, 3871–3878. (doi:10.1016/S0142-9612(02)00131-X)

Sun, H., Wu, C., Dai, K., Chang, J. & Tang, T. 2006 Proliferation and osteoblastic differentiation of human bone marrow-derived stromal cells on akermanite–bioactive ceramics. *Biomaterials* **27**, 5651–5657. (doi:10.1016/j.biomaterials.2006.07.027)

Vrouwenvelder, W. C. A., Groot, C. G. & de Groot, K. 1992 Behaviour of fetal rat osteoblasts cultured *in vitro* on bioactive glass and nonreactive glasses. *Biomaterials* **13**, 382–392. (doi:10.1016/0142-9612(92)90044-O)

Webb, K., Hlasy, V. & Tresco, P. A. 1998 Relative importance of surface wettability and charged functional groups on NIH 3T3 fibroblast attachment, spreading, and cytoskeletal organization. *J. Biomed. Mater. Res.* **41**, 422–430. (doi:10.1002/(SICI)1097-4636(19980905)41:3<422::AID-JBM12>3.0.CO;2-K)

Webster, T. J., Siegel, R. W. & Bizios, R. 1999 Osteoblast adhesion on nanophase ceramics. *Biomaterials* **20**, 1221–1227. (doi:10.1016/S0142-9612(99)00020-4)

Wei, J., Li, Y. & Lau, K-.T. 2007 Preparation and characterization of a nano apatite/polyamide$_6$ bioactive composite. *Compos. B: Eng.* **38**, 301–305. (doi:10.1016/j.compositesb.2006.05.006)

Weia, G. & Ma, P. X. 2004 Structure and properties of nano-hydroxyapatite/polymer composite scaffolds for bone tissue engineering. *Biomaterials* **25**, 4749–4757. (doi:10.1016/j.biomaterials.2003.12.005)

Wennerberg, A., Ektessabi, A., Albrektsson, T., Johansson, C. & Andersson, B. 1997 A 1-year follow-up of implants of differing surface roughness placed in rabbit bone. *Int. J. Oral Maxillofac. Implants* **12**, 486–494.

Wu, C., Chang, J., Zhai, W., Ni, S. & Wang, J. 2006*a* Porous akermanite scaffolds for bone tissue engineering: preparation, characterization, and *in vitro* studies. *J. Biomed. Mater. Res. B: Appl. Biomater.* **78**, 47–55.

Wu, C., Chang, J., Ni, S. & Wang, J. 2006*b* *In vitro* bioactivity of akermanite ceramics. *J. Biomed. Mater. Res. A* **76**, 73–80.

Xue, W., Liu, X., Zheng, X. & Ding, C. 2005 *In vivo* evaluation of plasma-sprayed wollastonite coating. *Biomaterials* **26**, 3455–3460. (doi:10.1016/j.biomaterials.2004.09.027)

Xynos, I. D., Edgar, A. J., Buttery, L. D. K., Hench, L. L. & Polak, J. M. 2000*a* Gene expression profiling of human osteoblasts following treatment with the ionic products of Bioglass 45S5 dissolution. *J. Biomed. Mater. Res. A* **55**, 151–157. (doi:10.1002/1097-4636(200105)55:2<151::AID-JBM1001>3.0.CO;2-D)

Xynos, I. D., Edgar, A. J., Buttery, L. D., Hench, L. L. & Polak, J. M. 2000*b* Ionic products of bioactive glass dissolution increase proliferation of human osteoblasts and induce insulin-like growth factor II mRNA expression and

protein synthesis. *Biochem. Biophys. Res. Commun.* **276**, 461–465. (doi:10.1006/bbrc.2000.3503)

Xynos, I. D., Hukkanen, M. V. J., Batten, J. J., Buttery, I. D., Hench, L. L. & Polak, J. M. 2000*c* Bioglass® 45S5 stimulates osteoblast turnover and enhances bone formation *in vitro*: implications and applications for bone tissue engineering. *Calcif. Tissue Int.* **67**, 321–329. (doi:10.1007/s002230001134)

Yang, M., Zhu, S., Chen, Y., Chang, Z., Chen, G., Gong, Y. & Zhao, N. 2004 Studies on bone marrow stromal cells affinity of poly(3-hydroxybutyrate-*co*-3-hydroxyhexanoate). *Biomaterials* **25**, 1365–1373. (doi:10.1016/j.biomaterials.2003.08.018)

Zhang, R. & Ma, P. X. 1999*a* Poly(alpha-hydroxyl acids)/hydroxyapatite porous composites for bone tissue engineering. I. Preparation and morphology. *J. Biomed. Mater. Res.* **44**, 446–455. (doi:10.1002/(SICI)1097-4636(19990315)44:4<446::AID-JBM11>3.0.CO;2-F)

Zhang, R. & Ma, P. X. 1999*b* Porous poly(L-lactic acid)/apatite composites created by biomimetic process. *J. Biomed. Mater. Res.* **45**, 285–293. (doi:10.1002/(SICI)1097-4636(19990615)45:4<285::AID-JBM2>3.0.CO;2-2)

Zhao, W. & Chang, J. 2005 Preparation and characterization of novel tricalcium silicate bioceramics. *J. Biomed. Mater. Res. A* **73**, 86–89.